# Theoretical profiles of the Mg + resonance lines perturbed by collisions with He

Nicole F. Allard, G. Guillon, V. A. Alekseev, J. F. Kielkopf

A&A 593, A13 (2016)
DOI: 10.1051/0004-6361/201628781


Astronomy & Astrophysics

# Theoretical profiles of the $Mg^+$ resonance lines perturbed by collisions with He

N. F. Allard[1,2], G. Guillon[3], V. A. Alekseev[4], and J. F. Kielkopf[5]

[1] GEPI, Observatoire de Paris, PSL Research University, UMR 8111, CNRS, Université Denis Diderot, Sorbonne Paris Cité, 61 avenue de l'Observatoire, 75014 Paris, France
e-mail: nicole.allard@obspm.fr
[2] Institut d'Astrophysique de Paris, UMR 7095, CNRS, Université Paris VI, 98bis boulevard Arago, 75014 Paris, France
[3] Laboratoire Interdisciplinaire Carnot de Bourgogne, UMR 6303, CNRS, Université de Bourgogne, 21078 Dijon Cedex, France
[4] St. Petersburg State University, 7/9 Universitetskaya Nab., 199034 St. Petersburg, Russia
[5] Department of Physics and Astronomy, University of Louisville, Louisville, Kentucky 40292, USA

Received 23 April 2016 / Accepted 4 June 2016

**ABSTRACT**

*Context.* The effects of collision broadening by He are central to understanding the opacity of cool stellar atmospheres.
*Aims.* DZ white dwarfs show metal lines which are, in many cases, believed to come from some rocky material, a remnant of a former exoplanetary system. The analysis of the $Mg^+$ resonance lines is a valuable method to determine the chemical abundances in these systems.
*Methods.* Unified profiles of the strongest of the UV lines of $Mg^+$ have been calculated in the semi-classical approach using very recent ab initio potential energies.
*Results.* We present the first theoretical line profile calculations of the resonance lines of $Mg^+$ that have been perturbed by helium in physical conditions of atmospheres in helium-rich white dwarfs with metal traces.

**Key words.** line: profiles – white dwarfs – stars: atmospheres

## 1. Introduction

He-rich white dwarfs with metals are classified as DBZ and, at low temperature, they are DZ. Recent key observations with *Spitzer* and *Hubble* space telescopes have given us real insights into the composition of extra-solar planetary systems through the spectroscopic detection of traces of heavy metal in cool DZ white dwarf atmospheres. These observed features are now attributed to the presence of rocky planetary material like asteroids that previously orbited these stars. They could play a central role in characterizing the chemistry of this rocky material. The analysis of DZ spectra is therefore a potentially valuable method for determining the existence in the stellar progenitor of exoplanetary systems and their chemical abundances (see Farihi 2016, and references therein).

The construction of model atmospheres and synthetic spectra for DZ white dwarfs is necessary to derive reliable atmospheric parameters and the surface chemical composition for these objects. In the absence of hydrogen, the effect of all other opacity sources on the structure of the atmosphere is significantly enhanced. The omission of opacity results in systematic errors in the predicted flux distribution and hence in the effective temperature. This is a major concern for the calculation of model atmospheres. Heber & Schoenberner (1981) introduced the blanketing effect of strong ultraviolet metal lines. The methods to include all the broadened lines remain misleading, a reliance on simplified models of van der Waals quasi-static line broadening (see Koester et al. 2011, and references therein). These recipes are widely in use in model atmospheres, the broadening constants $C_6$ being determined following Unsold (1955). As noted by Koester et al. (2011), Zeidler-K.T. et al. (1986) studied line blanketing and metal abundances in helium-rich white dwarf atmospheres. They noted that, with the low electron densities being present, line broadening is dominated by collision broadening with neutral He. Initial assumptions of $C_6$ based on the methods of Unsold (1955) and others led to inconsistencies in the model spectra, strikingly in the observed absence of weak Mg lines that should have been present at the abundances required to match the resonance lines. They found that, by artificially increasing $C_6$ by an order of magnitude, they could reproduce the observed spectra. However, even with that ad hoc choice, discrepancies in the core and wing of Mg II lines could not be removed.

The shift of the line arises from the long-range part of potentials and the far line wings of the broadened lines exhibit characteristics that arise at short range. In a first approximation, van der Waals potentials describe the long-range part of the potentials. However, it is most important that accurate molecular potentials be involved in the calculations of line broadening and opacities for radiative transitions. Line broadening of the $Ca^+$ and $Mg^+$ resonance lines in presence of He have been studied by Bottcher et al. (1975) and Monteiro et al. (1986) using model potential curves. In this work we consider the broadening of $Mg^+$ by He to develop an accurate treatment of the resonance lines, including the very far wing that enables correct calculations of radiative transport in DZ white dwarfs.

For that purpose, intensive ab initio calculations have been performed to obtain the ground and first excited potential energy curves (PECs) for the $Mg^+$–He system. We report and compare the results of two different methods to compute ab initio $Mg^+$He

interaction potentials (Sect. 2). A reliable determination of the line profiles that is applicable in all parts of the line at all densities is the Anderson semi-classical unified theory, which utilizes the Fourier transform of an autocorrelation function (Anderson 1952) (Sect. 3). This paper is a continuation of our studies of sodium and ionized Ca resonance lines perturbed by He (Allard 2013; Allard & Alekseev 2014; Allard et al. 2014a). We illustrate the evolution of the absorption spectra of $Mg^+$-He collisional profiles for the densities (Sect. 3.1) and the temperatures (Sect. 3.2) prevailing in the atmosphere of cool white dwarf stars. The calculations span the range 4000 K to 12 000 K. Moreover, the impact approximation determines the asymptotic behavior of the unified line shape autocorrelation function. The dependence of the impact line parameters on temperature is presented in Sect. 4. In this way, the results described here are applicable to a more general line profile and opacity evaluation for the same perturbers at any given layer in the photosphere.

## 2. $Mg^+$He diatomic potentials

Line profile intensities are functions of both excited and ground state interactions and consequently a precise determination of the electronic energies, as well as optical transition dipole moments, are crucial to compute accurate line profiles for the whole wavelength range. In this section, we report on and compare the results of two different methods to compute ab initio $Mg^+$He interaction potentials.

### 2.1. CASSCF-CASPT2 calculations

Calculations were performed by one of us (hereafter VA) using MOLCAS 7.6 (Aquilante et al. 2010). Energies with the inclusion of the static contribution of electron correlation energy were calculated at the CASSCF (complete active space self-consistent field) level. Calculations of the dynamic electron correlation effects for the multiconfigurational CASSCF wave functions are based on the second order perturbation theory, the CASPT2 method in MOLCAS (Finley et al. 1998). The CASSCF-CASPT2 energies and wave functions are further used to obtain adiabatic energies with the inclusion of the spin-orbit interaction using the state interaction program RASSI (restricted active space state interaction) in MOLCAS (Malmqvist et al. 2002). The RASSI program also calculates dipole moments of optical transitions between electronic states.

Calculations were performed using relativistic atomic natural orbital (ANO) type basis sets (Almlöf & Taylor 1987). The potentials shown in Fig. 1 were obtained with Mg.ano-rcc.Roos.17s12p6d2f2g.9s8p6d2f2g, He.ano-rcc.Widmark.9s4p3d2f.7s4p3d2f, which are the largest ANO-type basis sets in the MOLCAS basis set library. The accuracy of CASSCF-CASPT2-RASSI calculations with the ANO basis sets has been discussed in detail in Roos et al. (2004). Smaller ANO-type basis sets for the He atom (VQZP and VTZP) were tested as well. The deviations from the results obtained with the largest basis sets were found to be rather small (at least the differences would not be seen in the scale of Fig. 1). The asymptotic energies were adjusted to match the energies of the $Mg^+(3p^2P_{1/2,\,3/2})$ doublet.

Calculations were performed in the $C_1$ symmetry for an active space consisting of the five lowest in energy unoccupied orbitals, including the singly occupied valence $2p^6 3s$ orbital. This selection of active space yields electronic states of the $Mg^+$He molecule, which correlate with the ground $2p^6 3s$ and excited 3p and 4s states of the $Mg^+$ ion. The interaction of Mg $2p^6 3p$ with He provides $^2\Pi_{1/2,\,3/2}$ states, and a $^2\Sigma$ state. A slight difference between the $^2\Pi_{1/2}$ and $^2\Pi_{3/2}$ states is not seen in the scale of Fig. 1. The dipole moment of $3s^2\Sigma \rightarrow 3p^2\Pi$ transitions is nearly constant. The $3p^2\Sigma$ state interacts with a higher lying $4s^2\Sigma$ state. Owing to this interaction, the dipole moment of the resonance 3s $^2\Sigma \rightarrow$ 3 $p^2\Sigma$ transition decreases (Fig. 3), while the asymptotically forbidden $3s^2\Sigma^+ \rightarrow 4s^2\Sigma^+$ transition acquires some strength as $R$ decreases.

### 2.2. CASSCF-MRCI calculations

The improvement over the previous molecular data described above consists in a more accurate determination of the intermediate and long-range part of the $Mg^+$-He potential. The potential energy curves were computed over a large range of intermolecular distances, namely, from 2.0 to 200.0 au, allowing a good description of the spectral line core. This is important when determining the absorption spectra of $Mg^+$-He obtained at low He density. All new ab initio calculations have been performed by one of us (hereafter GG) using the MOLPRO package (Werner et al. 2012). The dimer ground state emerges from the ion $Mg^+$ itself in its ground state $[Ne]3s^1\ ^2P$ and has $\Sigma$ symmetry (noted $X\ ^2\Sigma$), while the lowest two excited states come from the first excited state of $Mg^+$. One has $\Pi$ symmetry (e.g. A $^2\Pi$) and presents a very deep and narrow well, at short range, and the other is of a pure anti-bonding type with $\Sigma$ symmetry (e.g. B $^2\Sigma$). We have computed adiabatic potential energy curves (PECs) for the ground state and the first two excited states of $Mg^+$ + He. To this end, we have used a high level ab initio method, namely the state-averaged complete active space self-consistent field-multireference configuration interaction (SA-CASSCF-MRCI).

In view of the small mass of Mg, all scalar relativistic effects have been neglected at this point. MRCI calculations based on reference functions obtained from the state-averaged complete active space self-consistent field (SA-CASSCF) method are performed to get the best possible accuracy on the first excited states' energies. The active space used in the SA-CASSCF method contains five $\sigma$-type and four $\pi$-type molecular orbitals. The former correlate asymptotically to the $Mg^+$:3s, $3p_0$ and He:1s, 2s, $2p_0$ atomic orbitals, the latter to the $Mg^+$:$3p_1$, $3p_{-1}$ and He:$2p_1$, $2p_{-1}$ atomic orbitals. All electrons were dynamically included in the calculations.

For the ion $Mg^+$, since a good description of the core is necessary, we used the core-valence aug-cc-pCVQZ basis set, which possesses additional tight functions, with contraction scheme (20s, 16p, 7d, 5f, 3g) $\longrightarrow$ (10s, 9p, 7d, 5f, 3g). To describe the He atom, we used the aug-cc-pV6Z basis set, formed using 186 primitive functions with contraction scheme (11s, 6p, 5d, 4f, 3g, 2h) $\longrightarrow$ [7s, 6p, 5d, 4f, 3g, 2h]. The use of such an extended basis set is expected to provide results for atomic and molecular properties very close to the complete basis set limit and to dramatically reduce the basis set superposition errors, which have already been corrected with the usual counterpoise method (Boys & Bernardi 1970). To correct for the lack of size-consistency of the MRCI method, we used the Davidson cluster-corrected total energies (Davidson & Silver 1977) within the realm of the supermolecule approach to obtain complexation energies.

The ab initio data points obtained have been fitted to an RKHS kernel, as described in Ho & Rabitz (1996). These analytic forms of the adiabatic PECs allow a proper description of the long range part of the potential. In particular, the ground state

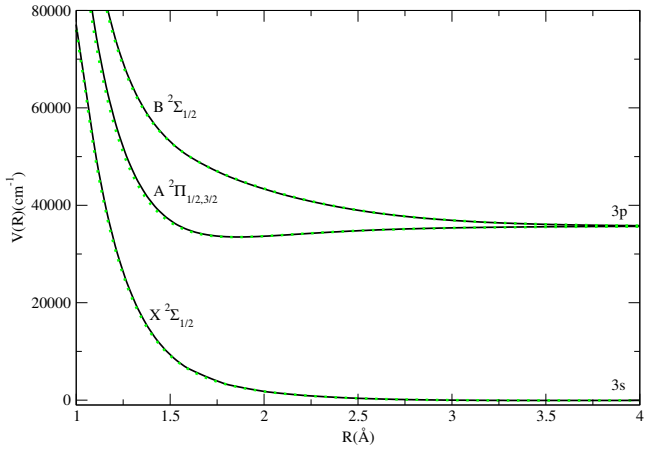


**Fig. 1.** Short-range part of the potential curves for the 3s and 3p states of the $Mg^+He$ molecule of GG (black lines) compared to VA (green dotted lines).

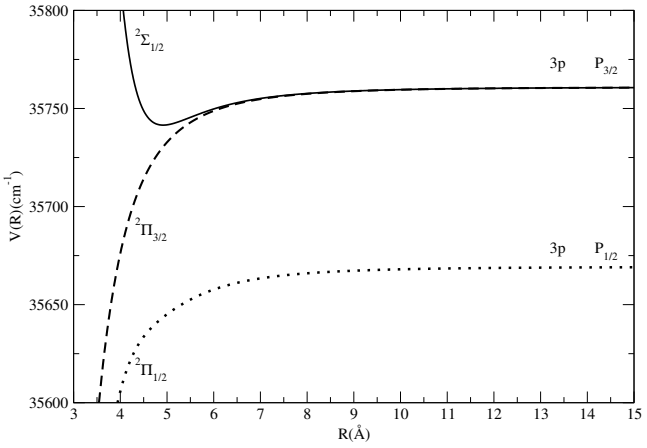


**Fig. 2.** Long range part of the GG potential curves correlated with 3p states. $^2\Sigma_{1/2}$ (full line), $^2\Pi_{3/2}$ (dashed line) and $^2\Pi_{1/2}$ (dotted line).

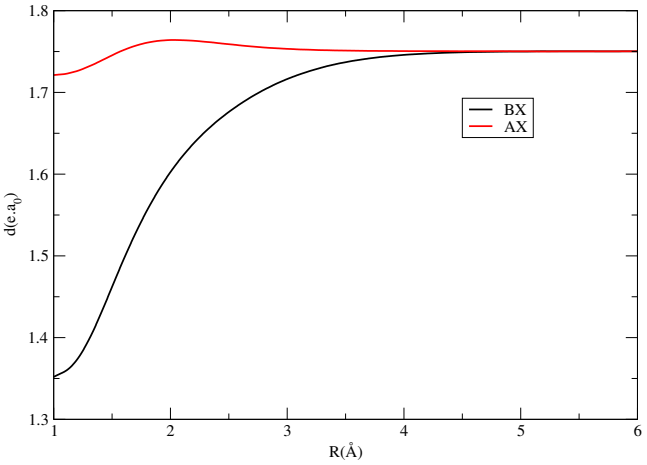


**Fig. 3.** Dipole moments for the $3\,s \rightarrow 3\,p$ transitions in $Mg^+He$ molecule (CASSCF–CASPT2 calculations).

interaction of $Mg^+He$ is correctly described as behaving asymptotically in $r^{-4}$, as it should for a charge-induced dipole system.

The electrostatic interaction between $Mg^+$ and He is much stronger than that between Mg and He, owing to the ionic character of $Mg^+$, with a well for the ground state roughly 14 times deeper than that of its neutral conterpart MgHe. As a result, the $X\ ^2\Sigma$ state presents a well depth $D_e$ of roughly $-68.0$ cm$^{-1}$ at an internuclear distance $r_e = 6.7$ a.u., which are values close to those obtained earlier ($D_e = -73.2$ cm$^{-1}$ and $r_e = 6.6$ a.u.) by Gardner et al. (2010). The $A^2\Pi$ state exhibits a narrow well 2267 cm$^{-1}$ deep at $r_e = 3.5$ a.u.

Also, the Russel-Saunders spin-orbit coupling in the ion $Mg^+$ ($\Delta_{SO} = 91.57$ cm$^{-1}$) is comparable to that of the Na atom ($\Delta_{SO} = 17.20$ cm$^{-1}$) (Dell'Angelo et al. 2012; Allard et al. 2014b), but still roughly five times larger. However, we make the hypothesis that the effect of the value of the atomic $Mg^+$ spin-orbit coupling parameter $\Delta_{SO}$ only varies slowly when the $Mg^+$ ion and He atom approach one another. In this way, we avoid computations of its variation with internuclear distance, which could be done using relativistic electronic structure calculations, or at least relativistically-based corrections. The incorporation of the Russel-Saunders $Mg^+$ spin-orbit coupling at all internuclear distances, starting from the adiabatic PECs, is then realized following the lines described in Cohen & Schneider (1974).

Figures 1 and 2 show the potential energy curves obtained with MRCI calculations, which will be used in the line profile calculations presented in the paper.

$$V_e[R(t)] = E_e[R(t)] - E_e^{\infty}. \quad (1)$$

The potentials obtained in CASPT2 and MRCI calculations are overplotted in Fig. 1. As can be seen, the results of these two methods are in a good agreement at short internuclear distance.

## 3. Absorption spectra for cool white dwarfs

In a previous paper (Allard et al. 1999), we derived a classical path expression for a pressure-broadened atomic spectral line shape that allows for an electric dipole moment that is dependent on the position of perturbers, which is not included in the more usual approximation of Anderson (1952) and Baranger (1958b,a). When broadened by helium, absorption coefficients of ionized magnesium resonance lines arising from 3s to 3p transition depend on di-molecule potentials composed of $Mg^+$ and He (Figs. 1, 2) and dipole moments (Fig. 3).

The spectrum, $I(\Delta\omega)$, is the Fourier transform (FT) of the dipole autocorrelation function, $\Phi(s)$. This is given by

$$I(\Delta\omega) = \frac{1}{\pi} Re \int_0^{+\infty} \Phi(s) e^{-i\Delta\omega s} ds. \quad (2)$$

A pairwise additive assumption allows us to calculate $I(\Delta\omega)$, when $N$ perturbers interact as the FT of the $N$th power of the autocorrelation function $\phi(s)$ of a unique atom-perturber pair. For a perturber density $n_p$, we obtain

$$\Phi(s) = e^{-n_p g(s)}, \quad (3)$$

where the decay of the autocorrelation function with time leads to atomic line broadening.

For a transition $\alpha = (i, f)$ from an initial state $i$ to a final state $f$, we have

$$g_\alpha(s) = \frac{1}{\sum_{e,e'}{}^{(\alpha)} |d_{ee'}|^2} \sum_{e,e'}^{(\alpha)} \times \int_0^{+\infty} 2\pi\rho d\rho \int_{-\infty}^{+\infty} dx\, \tilde{d}_{ee'}[R(0)] \times [e^{\frac{i}{\hbar}\int_0^s dt\, V_{e'e}[R(t)]}\, \tilde{d}^*_{ee'}[R(s)] - \tilde{d}_{ee'}[R(0)]]. \quad (4)$$

In Eq. (4), $e$ and $e'$ label the energy surfaces on which the interacting atoms approach the initial and final atomic states of

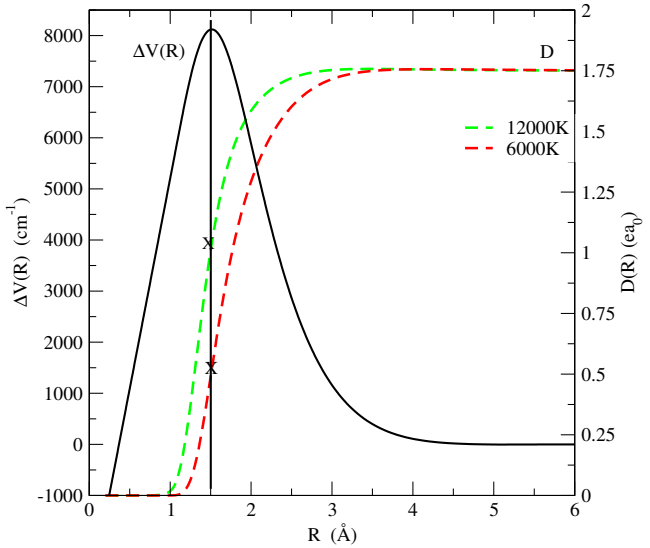


**Fig. 4.** Variation with temperature in the modulated dipole and the difference potential of the $B$-$X$ states of $Mg^+$-He molecule.

the transition. The sum $\sum_{e,e'}^{(\alpha)}$ is over all pairs $(e, e')$ such that $\omega_{e',e}(R) \to \omega_\alpha$ as $R \to \infty$.

For a more direct comparison of the contributions of the two fine-structure components of the doublet, it is convenient to use a cross-section $\sigma$ associated with each component. The relationship between the computed cross-section and the normalized absorption coefficient given in Eq. (2) is

$$I(\Delta\omega) = \sigma(\Delta\omega)/\pi r_0 f, \tag{5}$$

where $r_0$ is the classical radius of the electron, and $f$ is the oscillator strength of the transition.

In the sections which follow, we review the meaning of these terms in Eq. (4) and the data we use to evaluate the absorption line shape of ionized magnesium resonance lines in dense helium.

### 3.1. Satellite bands and density dependence

In the present context, the perturbation of the frequency of the atomic transition during the collision results in a phase shift, $\eta(s)$, which is calculated along a classical path $R(t)$ that is assumed to be rectilinear. The phase shift

$$\eta(s) = \frac{i}{\hbar}\int_0^s \mathrm{d}t\; V_{e'e}[\,R(t)\,], \tag{6}$$

where $\Delta V(R)$ represents the difference between the electronic energies of the quasimolecular transition. The potential energy for a state $e$ is

$$V_e[R(t)] = E_e[R(t)] - E_e^\infty. \tag{7}$$

$$\Delta V(R) \equiv V_{e'e}[R(t)] = V_{e'}[R(t)] - V_e[R(t)]. \tag{8}$$

At time $t$ from the point of closest approach

$$R(t) = \left[\rho^2 + (x + \bar{v}t)^2\right]^{1/2}, \tag{9}$$

with $\rho$ the impact parameter of the perturber trajectory and $x$ the position of the perturber along its trajectory at time $t = 0$.

We see from the potentials in Fig. 2 that two excited molecular levels, $^2\Sigma_{1/2}$ and $^2\Pi_{3/2}$, contribute to the $P_{3/2}$ line and that

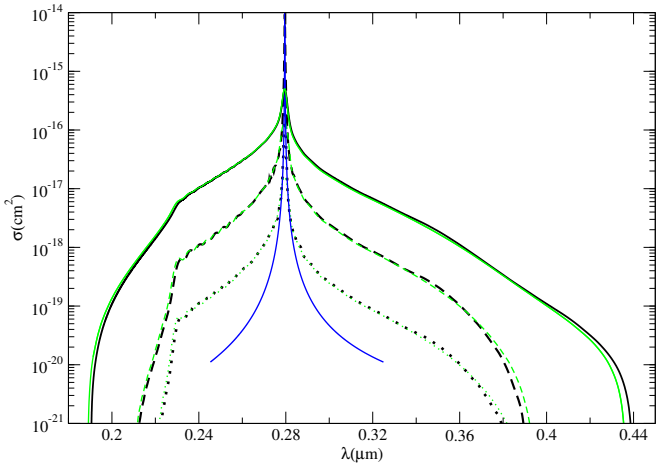


**Fig. 5.** Variation with He atom density of the $P_{3/2}$ component at $T$ = 6000 K. GG potentials (black curves), VA potentials (green curves). From top to bottom $n_{He} = 10^{22}$, $10^{21}$, and $10^{20}$ cm$^{-3}$. The corresponding Lorentzian profile for $n_{He} = 10^{20}$ cm$^{-3}$ is overplotted (blue line).

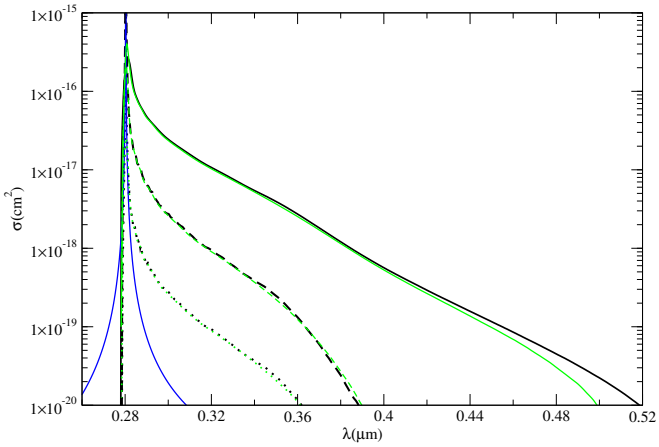


**Fig. 6.** Variation with He atom density of the $P_{1/2}$ component at $T$ = 6000 K. GG potentials (black curves), VA potentials (green curves). From top to bottom $n_{He} = 10^{22}$, $10^{21}$, and $10^{20}$ cm$^{-3}$. The corresponding Lorentzian profile for $n_{He} = 10^{20}$ cm$^{-3}$ is overplotted (blue line).

they produce opposite wings (Fig. 5). The $^2\Pi_{1/2}$ state that determines the $P_{1/2}$ line radiates solely in the red wing, and as a consequence the $P_{1/2}$ line, is strongly asymmetric to the red (Fig. 6).

Owing to the interaction between $Mg^+$ and He atoms, the far line wings of the broadened lines exhibit characteristics of molecular spectra. The potential difference $\Delta V$ related to the 3s $^2\Sigma_{1/2} \to$ 3p $^2\Sigma_{1/2}$ transition, for the $Mg^+$-He pair, has a maximum $\Delta V_{max}$ = 8100 cm$^{-1}$ at very short distance $R$ = 1.5 Å (Fig. 4). The unified theory (Anderson 1952; Allard 1978; Royer 1978) predicts that there will be quasi-molecular line satellites centered periodically at frequencies corresponding to the extrema of the difference potential. In the far blue wing, a notable feature is the primary peak that occurs at 0.23 $\mu$m (Fig. 5), corresponding to that large maximum of $\Delta V$. While, in the case of the triplet 3p−4s Mg lines, a satellite band located in the near blue wing is responsible of a blue asymmetry of the core of the lines. This asymmetry is a consequence of lower maxima (400 cm$^{-1}$) in the corresponding Mg-He potential energy difference curves (Leininger et al. 2015; Allard et al. 2016a).

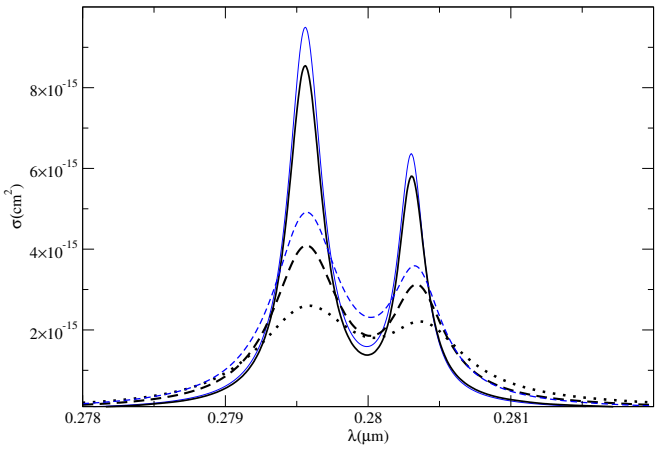


**Fig. 7.** Variation of the absorption cross-section in the central part of the sum of the components $P_{3/2}$ and $P_{1/2}$ with the He density, (from top to bottom $n_{He} = 1, 2$ and, $3 \times 10^{21}$ cm$^{-3}$, $T = 8000$ K). The corresponding sum of Lorentzian profiles for $n_{He} = 1$ and, $2 \times 10^{21}$ cm$^{-3}$ is overplotted (blue lines).

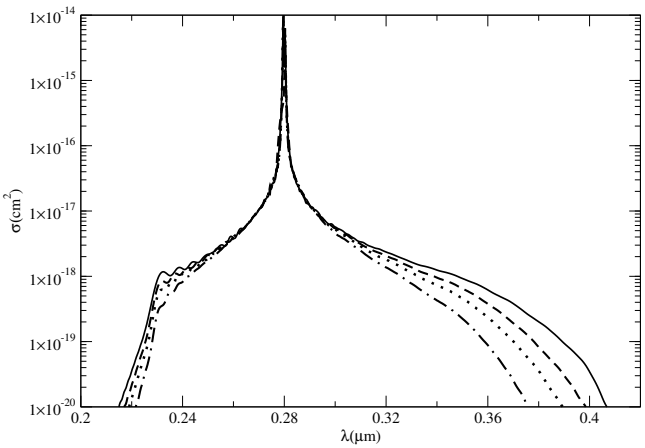


**Fig. 8.** Variation of the absorption cross-section of the sum of the components $P_{3/2}$ and $P_{1/2}$ with temperature, (from top to bottom $T = 12\,000$, 8000, 6000 and 4000 K, $n_{He} = 10^{21}$ cm$^{-3}$).

If one assumes additive-pair interactions, the satellite feature at $\Delta V_{max}$ in the binary spectrum will also appear in the spectrum at integer multiples of $\Delta V_{max}$ owing to the presence of additional perturbers in the collision volume $\mathcal{V}_{coll}$. When the helium density reaches $10^{21}$ cm$^{-3}$, a second satellite corresponding to $2\Delta V_{max}$ appears as a shoulder (Fig. 5). The blue wing of the $P_{1/2}$ component decreases very rapidly because of the shape of the potential of the A $^2\Pi_{1/2}$ state. While the red wings of the two components $P_{1/2,3/2}$ extend until 1200 Å and more from the line center for the helium density greater than $10^{21}$ cm$^{-3}$, the line wings are mostly formed in the lower photosphere, where higher helium density should prevail. At these high densities, the one-perturber binary collision approximation is not valid because the probability of an $Mg^+$ collision with two perturbers is larger than the probability of a collision with only one (Allard 1978; Royer 1978; Kielkopf & Allard 1979). The density effect on the core of the lines is also very significant when the He density becomes larger than $10^{21}$ cm$^{-3}$. Figure 7 shows that the Lorentzian gives a rather good description of the core until $n_{He} = 10^{21}$ atoms cm$^{-3}$, when the density is as high as $n_{He} = 2 \times 10^{21}$, the impact approximation is no more valid, even in the core of the line. The line shapes of the core of the doublet are no longer Lorentzian. The line parameters of the Lorentzians plotted in Figs. 5–7 are obtained in the impact approximation (see Sect. 4) using new ab initio potentials (Figs. 1 and 2).

A comparison of the absorption cross-sections for 3s−3p $P_{3/2}$ and 3s−3p $P_{1/2}$ transitions computed using VA potentials are shown in Figs. 5, 6. The agreement of the molecular data at short distance (Fig. 1), mainly in the slope of the repulsive walls, leads to this close agreement in the line wings and the prediction of the quasi-molecular line satellite at 0.23 $\mu$m. In Allard et al. (2007c), we have shown that ab initio K-$H_2$ potentials systematically less repulsive than the pseudo-potentials of Rossi & Pascale (1985) allowed a K-$H_2$ quasi-molecular line satellite to be predicted, which closely matches the position and shape of an observed feature in the spectrum of the T1 dwarf $\varepsilon$ Indi Ba (Allard et al. 2007a). More recently, in Allard et al. (2016b), the position of the predicted line satellite was confirmed by a laboratory measurement.

### 3.2. Temperature dependence

In Fig. 8 we show the absorption cross-section for the sum of the components of the resonance line of $Mg^+$ for a He density of $10^{21}$ cm$^{-3}$ and temperatures from 4000 to 12 000 K. The strength and extension of the line wings are very temperature sensitive. In Eq. (4) we define $\tilde{d}_{ee'}(R(t))$ as a modulated moment dipole (Allard et al. 1999)

$$D(R) \equiv \tilde{d}_{ee'}[R(t)] = d_{ee'}[R(t)]e^{-\frac{\beta}{2}V_e[R(t)]}, \quad (10)$$

where $\beta$ is the inverse temperature $(1/kT)$. The transition dipole moments $d_{ee'}(R)$ have been calculated by VA (Fig. 3). Here $V_e$ is the ground state potential X $^2\Sigma$ because we consider absorption transitions from the lower molecular state. The strength of the line satellite at about 0.23 $\mu$m increases with temperature (Fig. 8). The line wing amplitude depends on the value of the electric transition dipole moment in the internuclear region where the line wing is formed. In particular the presence and amplitude of line satellites are very sensitive to the temperature owing to the fast variation of the modulated dipole moment with temperature in the internuclear region, where the line satellite is formed (Fig. 4). This explains why the second line satellite appears distinctly at 12 000 K as a change in the slope on the blue wing.

From this dependence, it is apparent that the sensitivity of the line wings to pressure and temperature is a tool for determining basic parameters of white dwarf atmospheres, provided that the physics underlying its formation is well described. In the next section, we examine the dependence of the line parameters on the temperature.

## 4. Line core parameters

Pressure broadening by helium is one of the major broadening mechanisms in the atmosphere of DZ white dwarfs. Since the resulting line profile in a model atmosphere calculation is the integration of the flux in all layers from the deepest to the uppermost, it is important that the centers are adequately represented, i.e. they can be non-Lorentzian at high densities of the innermost layers, while Lorentzian in the upper atmosphere. However, they are characterized by different widths than were predicted by the hydrogenic van der Waals approximation, which is usually used for the cores, as was emphasized by Allard et al. (2007b)

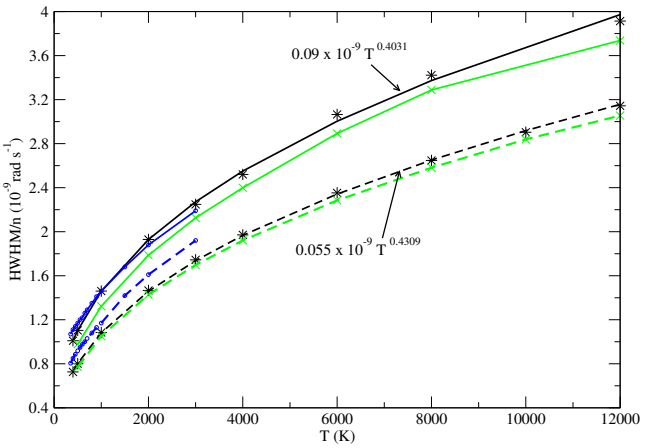


**Fig. 9.** Variation with temperature of the half-width at half-maximum of the $3P_{3/2}$–3s (full line) and $3P_{1/2}$–3s (dashed line) resonance lines of $Mg^+$ perturbed by He collisions. GG potentials (black curves), VA potentials (green curves), and model potentials of Monteiro et al. (1986; blue curves). The rates are in units of $10^{-9}$ rad $s^{-1}$.

and Peach (2011). At sufficiently low densities of perturbers, the symmetric center of a spectral line is Lorentzian and can be defined by two line parameters, the width and the shift of the main line. These quantities can be obtained in the impact limit ($s \to \infty$) of the general calculation of the autocorrelation function (Eq. (4)). For He density below $n_{He} = 10^{20}$ atoms $cm^{-3}$, the core of the line is described adequately by a Lorentzian (Figs. 5, 6). The line widths $w$ (HWHM) are linearly dependent on He density, and a power law in temperature given for the $^2P_{1/2}$ transition by

$$w = 0.055 \times 10^{-9} n_{He}\, T^{0.4309}, \quad (11)$$

and for the $^2P_{3/2}$ transition by

$$w = 0.09 \times 10^{-9} n_{He}\, T^{0.4031}. \quad (12)$$

The non-linear dependence on temperature is illustrated in Fig. 9. These expressions may be used to compute the widths for temperatures of stellar atmospheres from 400 to at least 12 000 K.

We are not aware of the laboratory measurements of spectra of $Mg^+$ under the conditions of high density and temperature needed for comparison with the calculations here. One set of experimental width and shift is available at lower temperature, $T = 556$ K by Giles & Lewis (1982) (Table 1). We undertook a comparison between calculated line parameters using different potentials and different theoretical approaches. In Fig. 9, we plotted the results obtained in the semi-classical unified theory using the VA potentials presented in Fig. 1. We notice that there is a rather good agreement of the results obtained with the GG potentials to those obtained by VA for the two components of the resonance line. Model potential curves for low-lying Σ and Π states of the $Ca^+$-He and $Mg^+$-He systems were calculated and used to obtain fully quantal broadening and shift parameters for the $Ca^+$ $4p\,^2P_{1/2,3/2}$–$4s\,^2S_{1/2}$ and $Mg^+$ $3p\,P_{1/2,3/2}$–$3s\,^2S_{1/2}$ spectral lines for a range of temperatures 400–3000 K. The broadening and shift parameters for $Mg^+$ and $Ca^+$ are given in Table 6 of Monteiro et al. (1986). In Fig. 9, we reported the temperature-dependence of the width of $Mg^+$ $3p\,P_{1/2,3/2}$–$3s\,^2S_{1/2}$. The widths were found to increase as $T^\alpha$, $\alpha$ taking the values 0.42 and 0.36 for the $Mg^+$ $P = 1/2$ and $P = 3/2$. A comparison between the experimental value at $T = 556$ K and the theoretical values is given in Table 1, with the experimental uncertainties given in brackets.

**Table 1.** Half-width at half maximum ($w$) and shift ($d$) ($10^{-9}$ rad $s^{-1}$) of the $P_{3/2}$ components at $T = 556$ K.

| Line parameters | Experiment[a] | Calculated[b] | Calculated[c] |
|---|---|---|---|
| $w$ | 1.79(0.19) | 1.20 | 1.15 |
| $d$ | −0.74(0.19) | −0.24 | −0.19 |

**Notes.** [(a)] Giles & Lewis (1982). [(b)] Monteiro et al. (1986). [(c)] This work (GG potentials).

This study shows the sensitivity of the line parameters to the potentials.

## 5. Conclusions

The atmospheres of DZ white dwarfs are almost pure helium. The accurate treatment of the $Mg^+$ resonance lines should strongly influence the predicted spectrum, as in the case of the triplet 3p–4s Mg lines (Allard et al. 2016a). This requires the knowledge of accurate line profiles under the physical conditions of the atmospheres of cool DZ white dwarfs. Many of the problems in collision-induced radiative transitions have been solved within the one-perturber approximation. At very low densities, the binary model for an optically active atom in collision with one perturber is valid for the whole profile, except for the central part of the line. In very cool white dwarfs, the perturber density $n_{He}$ is so high that the one-perturber approximation breaks down. When the He density is greater than $n_{He} = 10^{20}$ atoms $cm^{-3}$, the far wing of the $P_{3/2}$ and $P_{1/2}$ components of the resonance lines is due to multiple-perturber collisions, which are included in the theory and models described here. Experimental laboratory tests are planned to re-determine the low density and low temperature line core shift and width as a test of the long range potential. The test will also help identify distinctive characteristics of the line wings at high density as a test of the stronger, shorter range, interactions that are used for the theoretical models. In conclusion, complete unified line profiles based on accurate atomic and molecular physics should be incorporated into the analysis of cool DZ white dwarf spectra. They should provide a good fit of UV MgII resonance lines without an unphysical increase of the van der Waals constant $C_6$, as in Koester & Wolff (2000). Moreover the correct determination of the line parameters should allow a good description of the spectral line core.

## References


Allard, N. F. 1978, J. Phys. B: At. Mol. Opt. Phys., 11, 1383
Allard, N. F. 2013, in EAS Pub. Ser., 63, 403
Allard, N. F., & Alekseev, V. A. 2014, Adv. Space Res., 54, 1248
Allard, N. F., Royer, A., Kielkopf, J. F., & Feautrier, N. 1999, Phys. Rev. A, 60, 1021
Allard, F., Allard, N. F., Homeier, D., et al. 2007a, A&A, 474, L21
Allard, N. F., Kielkopf, J. F., & Allard, F. 2007b, EPJ D, 44, 507
Allard, N. F., Spiegelman, F., & Kielkopf, J. F. 2007c, A&A, 465, 1085
Allard, N. F., Homeier, D., Guillon, G., Viel, A., & Kielkopf, J. 2014a, J. Phys. Conf. Ser., 548, 012006
Allard, N. F., Nakayama, A., Stienkemeier, F., et al. 2014b, Adv. Space Res., 54, 1290
Allard, N. F., Leininger, T., Gadéa, F. X., Brousseau-Couture, V., & Dufour, P. 2016a, A&A, 588, A142
Allard, N. F., Spiegelman, F., & Kielkopf, J. F. 2016b, A&A, 589, A21
Almlöf, J., & Taylor, P. R. 1987, J. Chem. Phys., 86, 4070
Anderson, P. W. 1952, Phys. Rev., 86, 809
Aquilante, F., De Vico, L., Ferré, N., et al. 2010, J. Comput. Chem., 31, 224

Baranger, M. 1958a, Phys. Rev., 111, 494
Baranger, M. 1958b, Phys. Rev., 111, 481
Bottcher, C., Docken, K. K., & Dalgarno, A. 1975, J. Phys. B At. Mol. Phys., 8, 1756
Boys, S. F., & Bernardi, F. 1970, Mol. Phys., 19, 553
Cohen, J. S., & Schneider, B. 1974, J. Chem. Phys., 61, 3230
Davidson, E. R., & Silver, D. W. 1977, Chem. Phys. Lett., 52, 403
Dell'Angelo, D., Guillon, G., & Viel, A. 2012, J. Chem. Phys., 136, 114308
Farihi, J. 2016, New Astron. Rev., 71, 9
Finley, J., Malmqvist, P.-A., Roos, B. O., & Serrano-Andres, L. 1998, Chem. Phys. Lett., 288, 299
Gardner, A. M., Withers, C. D., Graneek, J. B., et al. 2010, J. Phys. Chem. A, 114, 7631
Giles, R. G., & Lewis, E. L. 1982, J. Phys. B At. Mol. Phys., 15, 2871
Heber, U., & Schoenberner, D. 1981, A&A, 102, 73
Ho, T., & Rabitz, H. 1996, J. Chem. Phys., 104, 2584
Kielkopf, J. F., & Allard, N. F. 1979, Phys. Rev. Lett., 43, 196
Koester, D., & Wolff, B. 2000, A&A, 357, 587
Koester, D., Girven, J., Gänsicke, B. T., & Dufour, P. 2011, A&A, 530, A114
Leininger, T., Gadéa, F. X., & Allard, N. F. 2015, in SF2A-2015: Proceedings of the Annual meeting of the French Society of Astronomy and Astrophysics, eds. F. Martins, S. Boissier, V. Buat, L. Cambrésy, & P. Petit, 397
Malmqvist, P., Roos, B. O., & Schimmelpfennig, B. 2002, Chem. Phys. Lett., 357, 230
Monteiro, T. S., Cooper, I. L., Dickinson, A. S., & Lewis, E. L. 1986, J. Phys. B At. Mol. Phys., 19, 4087
Peach, G. 2011, Balt. Astron., 20, 516
Roos, B. O., Lindh, R., Malmqvist, P.-A. K., Veryazov, V., & Widmark, P.-O. 2004, J. Phys. Chem. A, 108, 2851
Rossi, F., & Pascale, J. 1985, Phys. Rev. A, 32, 2657
Royer, A. 1978, Acta Phys. Pol. A, 54, 805
Unsold, A. 1955, Physik der Sternatmospharen, MIT besonderer Berucksichtigung der Sonne (Berlin: Springer)
Werner, H.-J., Knowles, P. J., Knizia, G., et al. 2012, MOLPRO, version 2012.1, a package of ab initio programs
Zeidler-K.T., E.-M., Weidemann, V., & Koester, D. 1986, A&A, 155, 356